Transport of colloids in saturated fractures

Constantinos V. Chrysikopoulos
Department of Civil and Environmental Engineering
University of California, Irvine, CA 92697-2175, USA
E-mail: costas@eng.uci.edu

Abstract

Analytical solutions for colloid transport in one-dimensional rock fractures with and without colloid penetration into the rock matrix are presented. These models idealize a single fracture as two semi-infinite parallel plates. Furthermore, the models assume that colloid particles undergo irreversible deposition onto fracture surfaces, may penetrate into the rock matrix, and deposit irreversibly onto rock-matrix solid surfaces. The impact of the model parameters on colloid transport is examined. Subsequently, a stochastic model for two-dimensional transient transport of colloids in a fracture-rock matrix system with spatially variable fracture aperture is presented. The aperture in the fracture plane is considered as a lognormally distributed random variable with spatial fluctuations described by an exponential autocovariance function. The fracture plane is partitioned into unit elements with different apertures generated stochastically from a lognormal distribution. Both equilibrium and kinetic colloid deposition onto fracture surfaces are investigated. Colloid surface exclusion is incorporated in the dynamics of kinetic deposition. The impact of deposited colloids on further colloid deposition is described by either a linear or a nonlinear blocking function. The governing transport equations are solved numerically for each realization of the aperture fluctuations. Simulated breakthrough curves of ensemble averages of several realizations show enhanced colloid transport and more pronounced fingering when colloids are subject to size exclusion from regions of small aperture size. Moreover, it is demonstrated that surface exclusion enhances colloid transport, and the assumption of clean bed media may underestimate liquid phase colloid concentrations.

1 Introduction

The possible leakage of canisters containing hazardous wastes and radioactive materials, which are often buried in deep fractured, low-permeability bedrocks, has motivated numerous studies of contaminant migration in fractured media (e.g., Neretnieks *et al.*, 1982; Abelin, 1986; Raven *et al.*, 1988; Krishnamoorthy *et al.*, 1992). Recent laboratory and field studies indicate that contaminants can migrate not only as dissolved species in the liquid phase, but also adsorbed on the surface of suspended colloid particles (e.g., Torok *et al.*, 1990; Buddemeier and Hunt, 1988; Chiou *et al.*, 1986). Puls and Powell (1992) concluded from laboratory experiments that iron oxide colloids may be mobile to a significant extent, and under some conditions these colloids may be transported faster than conservative tracers. Similar results were observed at the Nevada test site (Buddemeier and Hunt, 1988) and at a field experiment in crystalline fractured rocks (Champ and Schroeter, 1988). Because colloids have high surface area per unit mass, contaminants exhibit higher affinity for attachment onto colloids than onto solid surfaces (McDowell-Boyer *et al.*, 1986; Toran and Palumbo, 1992). Therefore, colloid particles serve as carriers for contaminants and may significantly influence the net rate of contaminant migration (Abdel-Salam and Chrysikopoulos, 1995a).

For reliable modeling of colloid transport in fracture networks, it is most important to thoroughly understand the main transport mechanisms within a single fracture. Various investigations have focused on the modeling of flow and contaminant transport in a single fracture (Neuzil and Tracy, 1981; Neretnieks, 1983; Novakowski *et al.*, 1985; Tsang and Tsang, 1987; Moreno *et al.*, 1988; Shapiro and Nicholas, 1989; Johns and Roberts, 1991; and Kessler and Hunt, 1994, to mention a few representative studies). A commonly used idealization of a natural single fracture is a pair of parallel plates separated by a constant aperture. The parallel plate model ignores the roughness, waviness, and tortuosity of the fracture surfaces (Schrauf and Evans, 1986). At high normal stresses caused by the overburden pressure, fracture surfaces tend to close, the contact area between these surfaces increases and consequently the fracture aperture becomes spatially dependent (Moreno *et al.*, 1988).

Colloids represent a class of very fine particles that generally range in size from 1 nm to 10 μm (see Figure 1); and they are named after the Greek word "$\kappa\acute{o}\lambda\lambda\alpha$," meaning "glue" (Russel *et al.*, 1989). Colloids present in subsurface formations are mainly mineral particles in the form of metal oxides, humic macromolecules, bacteria and viruses (Stumm and Morgan, 1981). In fractured media, colloids are formed by microerosion of minerals present in the subsurface matrix
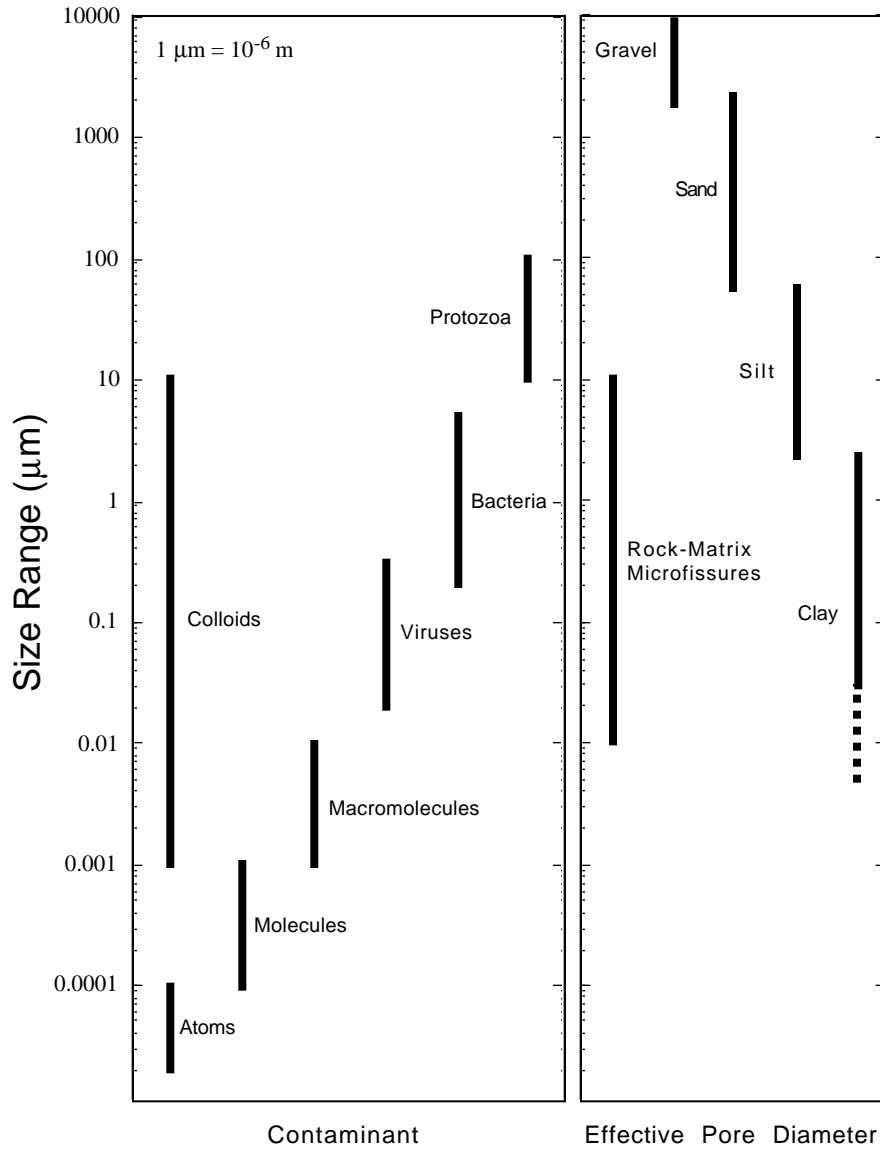
Figure 1: Size ranges of contaminants present in groundwater and effective pore diameters of various porous media, adopted from Chrysikopoulos and Sim (1996). Contaminant sizes are obtained from Stumm (1977), Matthess and Pekdeger (1981), and Buddemeier and Hunt (1988); microfissure sizes are obtained from Birgersson and Neretnieks (1982); effective pore diameters are calculated from average soil particle diameters reported by Mitchell (1976), by assuming a cubic packing: effective pore diameter = particle diameter $\times (\sqrt{2} - 1)$.

as a result of formation crushing due to tectonic activity (Drever, 1985). Colloid particles are also produced by the mechanical action of infiltrating water and chemical dissolution of rock matrix minerals. In addition, colloids form by changes in groundwater geochemical conditions such as pH, major element composition, redox potential, or partial pressures of CO_2 (McCarthy and Degueldre, 1993). Once a colloidal suspension is formed, it could be transported over significant distances. Suspended colloids are also subject to aggregation, filtration and settling, all of which are relatively complex processes dependent on colloid density, colloid size, surface chemistry, water chemistry, and interstitial velocity (McCarthy and Zachara, 1989). Colloids are found in subsurface waters under various geochemical conditions with concentrations ranging from a few milligrams per liter to a few hundred milligrams per liter (Moulin and Ouzounian, 1992). For instance, high particle concentration has been found in granitic rock fractures at the Nevada test site and in Switzerland (Buddemeier and Hunt, 1988; Mills *et al.*, 1991).

The transport of colloids is affected by hydrodynamic interactions between colloid particles, interstitial fluid, and fracture surfaces (Goldman *et al.*, 1967). The stability of colloids is an important consideration in determining their transport and is controlled by van der Waals attractive forces that promote aggregation, and electrostatic repulsive forces that keep particles apart. When electrostatic repulsions are dominant, colloid particles are electrostatically stabilized and remain in a dispersed state (McCarthy and Zachara, 1989). Conditions of weak electrostatic repulsive forces may promote coagulation which does not necessarily lead to immediate particle immobilization. Coagulation is a function of several variables, including particle concentration and particle size, which can influence the extent of particle–particle collisions. Moreover, destabilized colloids can still be transported as aggregates if the aggregates are sufficiently small relative to the fracture aperture.

As colloids are transported through fractures, they are subjected to sorption reactions with surrounding fracture surfaces. The adsorption of colloids onto solid surfaces is conventionally termed as filtration or deposition, while the desorption of colloids is known as detachment. A field experiment in crystalline rock fractures has demonstrated that the primary removal mechanism of bacterial and nonreactive colloids from the bulk solution is by deposition (Champ and Schroeter, 1988). Colloid deposition onto fracture surfaces can be characterized by either equilibrium or kinetic relationships. For mathematical simplicity many models for colloid transport in porous and fractured media incorporate a reversible, equilibrium deposition expression (Matthess *et al.*, 1988; Tim and

Mostaghimi, 1991; Grindrod, 1993; Smith and Degueldre, 1993; Chrysikopoulos and Sim, 1996). Kinetic colloid deposition models are based on the assumption that deposited colloids form either a monolayer coverage on the sorbent's surface when interparticle electrostatic forces prohibit contact of colloids (Adamczyk *et al.*, 1992) or a multilayer coverage when attractive electrostatic surface forces enhance particle–particle interactions (Ryde *et al.*, 1991). It should be noted, however, that charged colloid particles may cover less surface area of a sorbent than uncharged particles because the presence of intercolloidal forces hinder physical contact or overlapping between particles (Adamczyk *et al.*, 1994). The attachment of particles to the solid surface, or attachment efficiency, is the ratio of the rate at which particles attach to the solid surface to the rate at which particles strike the solid surface. Comprehensive compilations of particle deposition mechanisms have been presented by McDowell-Boyer *et al.* (1986), and McCarthy and Zachara (1989). Detachment of colloids is not expected in crystalline rocks where flow velocities are low. Bowen and Epstein (1979) have shown experimentally that the rate of release of deposited colloids from a smooth parallel-plate channel is negligible.

This chapter provides a set of analytical models for one-dimensional colloid transport in a single water saturated fracture. The effects of irreversible colloid deposition onto fracture surfaces, colloid penetration into the rock matrix, and irreversible colloid deposition onto rock-matrix solid surfaces on colloid transport are thoroughly described. Subsequently, the effect of colloid exclusion from areas of small aperture size on colloid transport is examined with a two-dimensional numerical model describing colloid transport within a saturated fracture with spatially variable aperture. Finally, the impact of some important equilibrium and kinetic colloid deposition mechanisms on colloid transport within a single fracture is investigated.

2 Analytical models for colloid transport

For a water saturated, one-dimensional fracture, as illustrated in Figure 2, the partial differential equation describing the transport of colloids under steady-state flow conditions, assuming that colloids may deposit irreversibly onto fracture surfaces, and may penetrate the rock matrix is given by

$$\frac{\partial n(t,x)}{\partial t} + \frac{2}{b}\frac{\partial n^*(t,x)}{\partial t} = D_{xx}\frac{\partial^2 n(t,x)}{\partial x^2}$$
$$- U_x\frac{\partial n(t,x)}{\partial x} + \frac{2\theta\mathcal{D}_e}{b}\frac{\partial n_m(t,x)}{\partial z}\bigg|_{z=b/2}, \qquad (1)$$
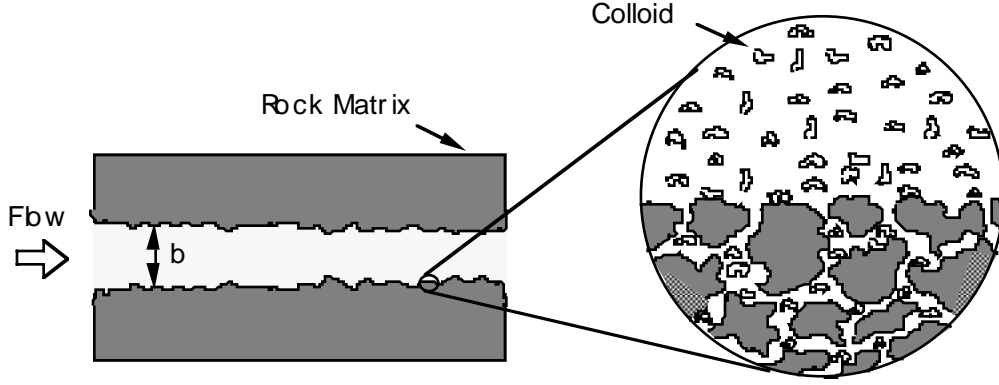
Figure 2: Illustration of a natural fracture represented by two parallel plates surrounded by the rock matrix. The mean aperture of the fracture is b. The suspended colloids can deposit onto the fracture surfaces and may diffuse into the rock matrix where the colloids can also deposit onto the rock matrix surfaces.

where n is the liquid-phase colloid concentration in the fracture; n^* is the concentration of colloids retained by deposition onto fracture surfaces expressed as mass of colloids per unit area of fracture surface; n_m is the colloid concentration in the rock matrix; D_{xx} is the dispersion coefficient for colloids; U_x is the average interstitial velocity in the fracture; $\mathcal{D}_e = \mathcal{D}/\tau^*$ is the effective diffusion coefficient for colloids (where $\mathcal{D}$ is the Brownian diffusion coefficient and $\tau^* > 1$ is the rock matrix tortuosity); b is the fracture aperture; θ is the porosity of the rock matrix; x is the coordinate along the fracture axis; z is the coordinate perpendicular to the fracture axis with origin at the center of the fracture; and t is time.

The mass flux of colloids onto fracture surfaces, represented by the second term on the left hand side of eqn (1), can be expressed as

$$\frac{\partial n^*(t,x)}{\partial t} = \frac{\kappa U_x}{b} n(t,x), \tag{2}$$

where κ is the fracture surface deposition coefficient, which is an experimentally determined "lumped" parameter that takes into account the different deposition mechanisms induced by Brownian motion, van der Waals and electric double layer forces. This relationship assumes that n^* is not affected by previously deposited particles on fracture surfaces. Similar relationships to eqn (2) for the filtration of colloids in porous media have been presented by Herzig *et al.* (1970) and Harvey

and Garabedian (1991); and in fractured media by Bowen and Epstein (1979), as well as Ibaraki and Sudicky (1995). However, in order to discriminate some inaccurate relationships previously presented in the literature, it should be noted that the mass flux of colloids onto fracture surfaces is inversely proportional to the fracture aperture, b.

The diffusive mass flux of colloids into the rock matrix is represented by the last term in eqn (1). The colloid concentration in the rock matrix, n_m, can be obtained from the following one-dimensional partial differential equation governing colloid diffusion in a direction perpendicular to the fracture axis, assuming that the interstitial liquid in the rock matrix is stationary, and that colloids deposit irreversibly onto rock-matrix solid surfaces

$$\frac{\partial n_m(t,x,z)}{\partial t} + \frac{\rho_b}{\theta}\frac{\partial n_m^*(t,x,z)}{\partial t} = \mathcal{D}_e\frac{\partial^2 n_m(t,x,z)}{\partial z^2}, \tag{3}$$

where n_m^* is the colloid concentration deposited on the rock matrix. Similar to colloid deposition onto fracture surfaces (eqn 2), the irreversible deposition of colloids onto rock-matrix solid surfaces can be expressed by the following linear kinetic relationship

$$\frac{\partial n_m^*(t,x,z)}{\partial t} = \frac{\kappa_m\theta}{\rho_b}n_m(t,x,z), \tag{4}$$

where κ_m is the rock matrix deposition coefficient. For a semi-infinite fracture and the presence of a continuous source of colloids, the appropriate initial and boundary conditions are:

$$n(0,x) = 0, \tag{5}$$

$$n(t,0) = n_o, \tag{6a}$$

$$-D_{xx}\frac{\partial n(t,0)}{\partial x} + U_x n(t,0) = U_x n_o, \tag{6b}$$

$$\frac{\partial n(t,\infty)}{\partial x} = 0, \tag{7}$$

$$n_m(0,x,z) = 0, \tag{8a}$$

$$n_m(t,x,b/2) = n(t,x), \tag{8b}$$

$$\frac{\partial n_m(t,x,\infty)}{\partial z} = 0, \tag{8c}$$

where n_o is the source colloid concentration. The condition (5) corresponds to the situation where colloids are initially absent from the one-dimensional fracture. The boundary condition (6a) represents the case of constant concentration

at the inlet; while the constant flux boundary condition (6b) implies colloid concentration discontinuity at the inlet. The downstream boundary condition (7) preserves concentration continuity for a semi-infinite fracture. The boundary condition (8b) implies equal concentration in the fracture and the rock matrix at the interface between them.

2.1 Without colloid penetration into the rock matrix

2.1.1 Constant concentration boundary condition

For the case of no colloid penetration into the rock matrix (i.e., $\partial n_m/\partial z=0$), and a constant concentration boundary condition, the analytical solution to eqns (1), (2), (5), (6a), and (7) is given by (Abdel-Salam and Chrysikopoulos, 1994)

$$n_{cc}(t,x) = \frac{n_o}{2}\left\{\exp\left[\frac{U_x x}{2D_{xx}}(1-\xi)\right]\mathrm{erfc}\left[\frac{x-U_x t\xi}{2(D_{xx}t)^{1/2}}\right]\right.$$

$$\left.+\exp\left[\frac{U_x x}{2D_{xx}}(1+\xi)\right]\mathrm{erfc}\left[\frac{x+U_x t\xi}{2(D_{xx}t)^{1/2}}\right]\right\}, \tag{9}$$

where

$$\xi = \left(1+\frac{8\kappa D_{xx}}{U_x b^2}\right)^{1/2}, \tag{10}$$

and the subscript cc indicates the use of the constant concentration upstream boundary condition. It should be noted that for the case of non-depositing colloid transport, κ is set to zero in the preceding equation.

2.1.2 Constant flux boundary condition

For the case of no colloid penetration into the rock matrix (i.e., $\partial n_m/\partial z=0$), and a constant flux inlet boundary condition, the analytical solution for eqns (1), (2), (5), (6b), and (7) is given by (Abdel-Salam and Chrysikopoulos, 1994)

$$n_{cf}(t,x) = n_o\left\{\frac{1}{1+\xi}\exp\left[\frac{U_x x}{2D_{xx}}(1-\xi)\right]\mathrm{erfc}\left[\frac{x-U_x t\xi}{2(D_{xx}t)^{1/2}}\right]\right.$$

$$+\frac{1}{1-\xi}\exp\left[\frac{U_x x}{2D_{xx}}(1+\xi)\right]\mathrm{erfc}\left[\frac{x+U_x t\xi}{2(D_{xx}t)^{1/2}}\right]$$

$$\left.+\frac{U_x b^2}{4D_{xx}\kappa}\exp\left[\frac{U_x x}{D_{xx}}-\frac{2U_x\kappa t}{b^2}\right]\mathrm{erfc}\left[\frac{x+U_x t}{2(D_{xx}t)^{1/2}}\right]\right\}, \tag{11}$$

where the subscript cf indicates the use of the constant flux upstream boundary condition. The preceding expression is valid only for $\kappa > 0$ which corresponds to $\xi > 1$. For the case of non-depositing colloid transport ($\kappa = 0$), the appropriate solution is (Lindstrom *et al.*, 1967; Gershon and Nir, 1969)

$$n_{cf}(t,x) = \frac{n_o}{2}\left\{ \text{erfc}\left[\frac{x - U_x t}{2(D_{xx}t)^{1/2}}\right] + \left(\frac{4U_x^2 t}{\pi D_{xx}}\right)\exp\left[-\frac{(x - U_{xx}t)^2}{4D_{xx}t}\right]\right.$$

$$\left. - \left(1 + \frac{U_x x}{D_{xx}} + \frac{U_x^2 t}{D_{xx}}\right)\exp\left[\frac{U_x x}{D_{xx}}\right]\text{erfc}\left[\frac{x + U_x t}{2(D_{xx}t)^{1/2}}\right]\right\}. \qquad (12)$$

2.2 Colloid penetration into the rock matrix

2.2.1 Constant concentration boundary condition

For the case of colloid penetration into the rock matrix (i.e., $\partial n_m/\partial z > 0$), and a constant concentration boundary condition, the analytical solution to eqns (1)–(6a), (7), and (8) was derived by Abdel-Salam and Chrysikopoulos (1994)

$$n_{cc_p}(t,x) = \frac{n_o}{\pi^{1/2}}\exp[B]\int_\ell^\infty \exp\left[-\eta^2 - \frac{Ex^2}{4D_{xx}\eta^2}\right]$$

$$\times\left\{ \exp\left[-\frac{\kappa_m x^2}{4D_{xx}\eta^2} - \frac{\kappa_m^{1/2}Ax^2}{4\eta^2}\right]\text{erfc}\left[\frac{Ax^2}{8\eta^2 T^{1/2}} - (\kappa_m T)^{1/2}\right]\right.$$

$$\left. + \exp\left[-\frac{\kappa_m x^2}{4D_{xx}\eta^2} + \frac{\kappa_m^{1/2}Ax^2}{4\eta^2}\right]\text{erfc}\left[\frac{Ax^2}{8\eta^2 T^{1/2}} + (\kappa_m T)^{1/2}\right]\right\}d\eta, \quad (13)$$

where the subscript cc_p indicates the use of the constant concentration upstream boundary condition with penetration into the rock matrix,

$$A = \frac{2\theta \mathcal{D}_e^{1/2}}{bD_{xx}}, \qquad (14)$$

$$B = \frac{U_x x}{2D_{xx}}, \qquad (15)$$

$$E = \frac{2\kappa U_x}{b^2} + \frac{U_x^2}{4D_{xx}} - \kappa_m, \qquad (16)$$

$$\ell = \frac{x}{2(D_{xx}t)^{1/2}}, \qquad (17)$$

$$T = t - \frac{x^2}{4D_{xx}\eta^2}, \qquad (18)$$

and η is a dummy integration variable.

2.2.2 Constant flux boundary condition

For the case of colloid penetration into the rock matrix (i.e., $\partial n_m/\partial z > 0$), and a constant concentration boundary condition, the solution to eqns (1)–(5), and (6b)–(8) is given by (Abdel-Salam and Chrysikopoulos, 1994)

$$n_{cf_p}(t,x) = \frac{n_o U_x}{2\pi D_{xx}^{1/2}} \exp\left[B - \kappa_m t\right]\left[f(t) * g(t)\right], \tag{19}$$

where the subscript cf_p indicates the use of the constant flux upstream boundary condition with penetration into the rock matrix; and $f * g$ is the convolution integral defined as

$$f(t) * g(t) = \int_0^t f(\tau)g(t - \tau) \, d\tau \tag{20}$$

where

$$f(t) = \int_\ell^\infty \exp\left[-\eta^2 - \frac{Ex^2}{4D_{xx}\eta^2}\right]$$

$$\times \left\{ \exp\left[\kappa_m T - \frac{\kappa_m^{1/2} Ax^2}{4\eta^2}\right] \mathrm{erfc}\left[\frac{Ax^2}{8\eta^2 T^{1/2}} - (\kappa_m T)^{1/2}\right]\right.$$

$$\left. + \exp\left[\kappa_m T + \frac{\kappa_m^{1/2} Ax^2}{4\eta^2}\right] \mathrm{erfc}\left[\frac{Ax^2}{8\eta^2 T^{1/2}} + (\kappa_m T)^{1/2}\right]\right\} d\eta \tag{21}$$

$$g(t) = \frac{1}{t^{3/2}}\left\{\int_0^\infty \exp\left[-\frac{\omega^2}{4t} - \omega(F + H)\right]\omega \, d\omega\right.$$

$$\left. - P^{1/2} \int_0^\infty \int_0^\omega \exp\left[-\frac{\omega^2}{4t} - H\omega - F(\omega^2 - \nu^2)^{1/2}\right] J_1\left[\nu P^{1/2}\right]\omega \, d\nu \, d\omega\right\}, \tag{22}$$

$$F = \frac{U_x}{2D_{xx}^{1/2}}, \tag{23}$$

$$H = \frac{AD_{xx}}{2}, \tag{24}$$

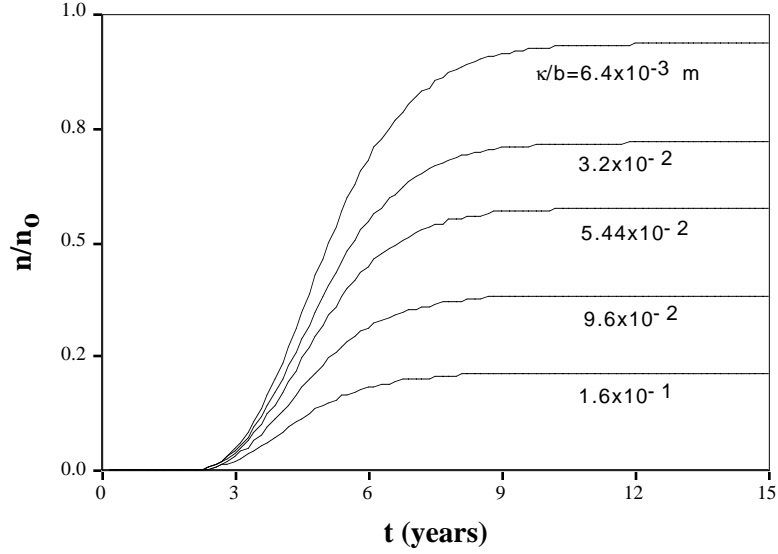$$P = E - \frac{A^2 D_{xx}^2}{4}, \tag{25}$$

Figure 3: Variation of the normalized liquid-phase colloid concentration with time for various values of the ratio of the fracture surface deposition coefficient to the fracture aperture squared as simulated by eqn (11) (here, D_{xx} =0.25 m^2/y, U_x =1.0 m/y, and $x = 5$ m).
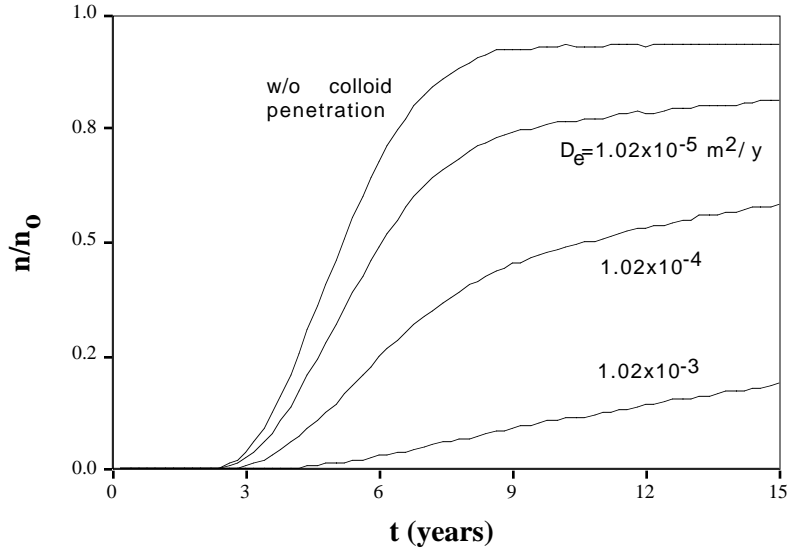

Figure 4: Variation of the normalized liquid-phase colloid concentration with time for various effective diffusion coefficient values as simulated by eqn (19) (here, b =1.25×10^{-4} m, D_{xx} =0.25 m^2/y, U_x =1.0 m/y, $x = 5$ m, κ =1.0×10^{-10} m, and κ_m =0 y^{-1}).

τ, ν, and ω are dummy integration variables; and J_1 is the modified Bessel function of the first kind of order one.

2.3 Model simulations

The parameter sensitivity and behavior of the one-dimensional colloid transport models presented here are investigated by several model simulations. The effect of the ratio of the fracture surface deposition coefficient, κ, to the fracture aperture squared, b^2, on the liquid-phase colloid concentration in the fracture as a function of time is presented in Figure 3. Clearly, the breakthrough curves indicate that increasing the deposition coefficient, while holding the fracture aperture constant, results in a reduction in the liquid-phase colloid concentration, because the deposition coefficient determines the amount of colloids to be deposited onto fracture surfaces. For a constant deposition coefficient the liquid-phase colloid concentration decreases with decreasing fracture aperture. This result is attributable to the fact that the smaller the fracture aperture the easier the access of colloid particles to fracture surfaces because of the shorter travel distance. It should be noted that the effect on liquid-phase colloid concentration due to an increase in the fracture aperture is exactly opposite to the resulting effect due to an increase in the deposition coefficient. Furthermore, the normalized concentrations of liquid-phase colloids as shown in Figure 3 do not reach the maximum value of one, because the models discussed here assume irreversible colloid deposition onto fracture surfaces.

Simulated breakthrough curves as well as snapshots for various parameter values indicate that the solutions presented by eqns (9) and (11) as well as eqns (13) and (19) exhibit similar behavior at low dispersion coefficients and high interstitial velocities. It should be noted that the boundary conditions (6a) and (6b) are approximately equivalent when D is negligible. At high interstitial velocity the advective flux in (6b) dominates over the dispersive flux, and thus there is no essential difference between the two boundary conditions. Consequently, the analytical solutions corresponding to the two boundary conditions examined become equivalent. Furthermore, Abdel-Salam and Chrysikopoulos (1994) have shown that the constant concentration inlet boundary condition overestimates the liquid-phase colloid concentrations, whereas the constant flux leads to conservation of mass. Similar results have been reported by van Genuchten and Parker (1984), and Leij *et al.* (1991) for certain cases of contaminant transport in saturated porous formations.

Model simulations based on eqn (19) with three different effective diffusion coefficients representing colloid particle diameters of 1, 0.1, and 0.01 μm, and rock matrix tortuosity τ^* of 1.33, are presented in Figure 4. The model simulations are also compared to the corresponding case of colloid transport without colloid penetration into the rock matrix. The predicted breakthrough curves demonstrate that an increase in the effective diffusion coefficient, or alternatively a decrease in particle size, leads to an increase in the colloid mass flux into the rock matrix and consequently to a decrease in the liquid-phase colloid concentration in the fracture. Also, the required time for colloid breakthrough increases with increasing effective diffusion coefficient. Furthermore, additional model simulations verify the intuitive result that an increase in the rock matrix deposition coefficient (κ_m), leads to a decrease in the colloid concentration in the rock matrix (n_m).

3 Transport of colloids in a saturated fracture with spatially variable aperture

Consider a two–dimensional, fully water-saturated fracture plane partitioned into 80×40 equal-size unit elements in the x and y directions, respectively, as shown in Figure 5. Each element exhibits a constant aperture. The aperture field in the fracture is generated stochastically by the geostatistical code COVAR (Williams and El-Kadi, 1986), assuming that the fracture aperture is a stationary stochastic variable with a known probability density function and spatial correlation length. It is assumed that the aperture distribution in the fracture plane follows a lognormal distribution with a mean of 1.65 μm and a standard deviation of 0.45 μm, and varies spatially according to an isotropic exponential autocovariance function with correlation length of 0.3 m. The aperture size ranges from 3 μm to 200 μm. These parameter values are approximately equal to those used by Moreno *et al.* (1988). The assumption of lognormally distributed aperture fluctuations is in agreement with measured apparent apertures from selective cores and well logs (Bianchi and Snow, 1968), apertures derived from permeability tests in granite (Bourke *et al.*, 1985), and aperture measurements of laboratory core samples (Gale, 1982; Hakami and Barton, 1990).
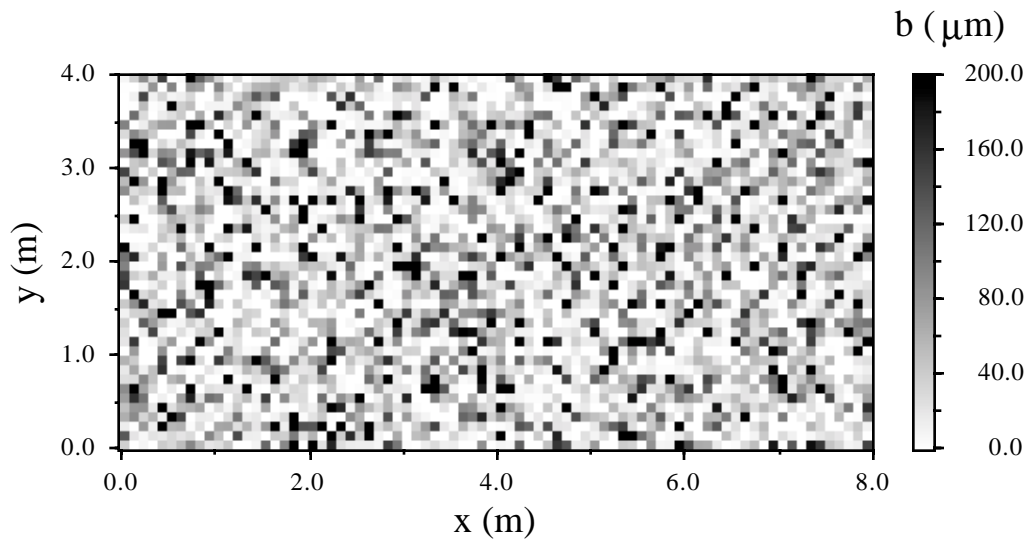
Figure 5: Schematic illustration of the two-dimensional fracture considered here. The fracture is partitioned into 80×40 equal-size elements. The gray scale represents aperture sizes.
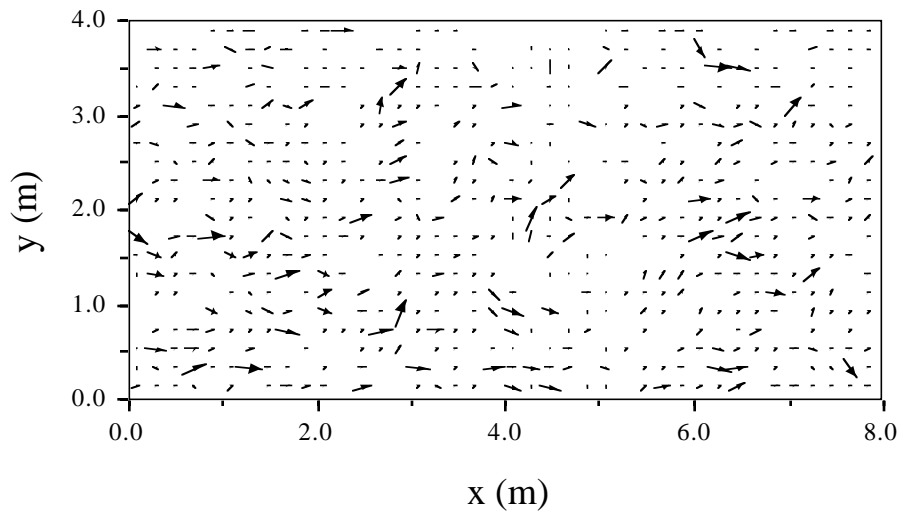

Figure 6: Velocity vector field in the fracture plane corresponding to a single realization of the aperture field. Arrow lengths are proportional to velocity magnitudes.

3.1 Mathematical model for a two-dimensional fracture

An appropriate partial differential equation describing the transport of colloids in a two-dimensional fracture with spatially variable aperture, assuming that colloids are stable of equal size and may deposit onto fracture surfaces but do not penetrate the rock matrix surrounding the fracture, is expressed as follows (Abdel-Salam and Chrysikopoulos, 1995b)

$$b(x,y)\frac{\partial n(t,x,y)}{\partial t} + 2\frac{\partial n^*(t,x,y)}{\partial t}$$
$$= \nabla \cdot \left[b(x,y)\mathbf{D} \cdot \nabla n(t,x,y) - b(x,y)\mathbf{U}n(t,x,y) \right], \quad (26)$$

where b is the fracture aperture; n is the concentration of colloids suspended in the liquid phase; n^* is the concentration of colloids deposited onto fracture surfaces, expressed as mass of colloids per unit area of the fracture surface; x is the coordinate along the fracture length; y is the coordinate along the fracture width; t is time; ∇ is the two-dimensional vector operator (del); $\nabla\cdot$ denotes divergence ($\nabla \cdot \mathbf{F} = \partial F_x/\partial x + \partial F_y/\partial y$, where $\mathbf{F}$ is an arbitrary two-dimensional vector); $\mathbf{U}$ is the interstitial fluid velocity vector defined as

$$\mathbf{U} = \begin{pmatrix} U_x(x,y) \\ U_y(x,y) \end{pmatrix}, \quad (27)$$

where U_x and U_y are the components of the interstitial velocity in the x and y directions, respectively; and $\mathbf{D}$ is a 2×2 symmetric matrix of hydrodynamic dispersion coefficients

$$\mathbf{D} = \begin{pmatrix} D_{xx}(x,y) & D_{xy}(x,y) \\ D_{yx}(x,y) & D_{yy}(x,y) \end{pmatrix}, \quad (28)$$

which can be determined from the velocity field by employing the following expression (Bear and Verruijt, 1987)

$$D_{ij}(x,y) = \alpha_T \delta_{ij}|\mathbf{U}| + \left(\alpha_L - \alpha_T\right)\frac{U_i(x,y)\,U_j(x,y)}{|\mathbf{U}|} + \mathcal{D}, \quad (29)$$

where α_L and α_T are the longitudinal and transverse dispersivities in the x and y directions, respectively; δ_{ij} is the Kronecker delta ($\delta_{ij} = 0$ for $i \neq j$ and $\delta_{ij} = 1$ for $i = j$) with subscripts $ij = xx$, xy, yx, or yy; and $|\mathbf{U}| = (U_x^2 + U_y^2)^{1/2}$

is the magnitude of the interstitial velocity vector. The velocity vector is two-dimensional because fracture aperture variability leads to a nonuniform velocity field. The governing transport eqn (26) assumes that no colloid mass is lost due to particle straining (entrapment between the fracture surfaces), and does not account for colloid diffusion into the rock matrix surrounding the fracture. As discussed in Section 2.3 of this chapter, colloid penetration into the rock matrix simply leads to a decrease in the liquid phase colloid concentration in the fracture.

The necessary initial and boundary conditions imposed on the two-dimensional fracture for the colloid transport model are as follows

$$n(0, x, y) = 0, \tag{30}$$

$$n(t, 0, y) = n_o, \tag{31}$$

$$\frac{\partial n(t, \ell_x, y)}{\partial x} = 0, \tag{32}$$

$$-D_{yy}(x, 0) \frac{\partial n(t, x, 0)}{\partial y} + U_y(x, 0)\, n(t, x, 0) = 0, \tag{33}$$

$$-D_{yy}(x, \ell_y) \frac{\partial n(t, x, \ell_y)}{\partial y} + U_y(x, \ell_y)\, n(t, x, \ell_y) = 0, \tag{34}$$

where ℓ_x and ℓ_y are the fracture dimensions in the x and y directions, respectively; and n_o is the constant colloid concentration at the source. The condition (30) establishes that there is no initial concentration of colloids suspended in the liquid phase. The constant concentration boundary condition (31) implies colloid concentration continuity at the upstream boundary. Equation (32) imposes the condition that the dispersive flux of colloids is zero and that concentration continuity is preserved at the downstream boundary. Furthermore, the conditions (33) and (34) imply that the lower and upper boundaries of the two-dimensional fracture are impervious to advective as well as dispersive transport of colloids.

The velocity components in the x and y directions at any location within the fracture are obtained by the following expression (de Marsily, 1986)

$$
\begin{aligned}
U_x(x, y) &= -K_f(x, y) \frac{\partial h(x, y)}{\partial x} \\
&= -\frac{\gamma b^2(x, y)}{12\mu} \frac{\partial h(x, y)}{\partial x},
\end{aligned} \tag{35}
$$

$$U_y(x, y) = -K_f(x, y)\frac{\partial h(x, y)}{\partial y}$$

$$= -\frac{\gamma b^2(x, y)}{12\mu}\frac{\partial h(x, y)}{\partial y}, \tag{36}$$

where h is the total head potential; $K_f = \gamma b^2/12\mu$ is the hydraulic conductivity of the fracture; γ is the specific weight of the interstitial fluid; and μ is the dynamic viscosity of the interstitial fluid.

The distribution of the total head potential within the fracture is obtained by the following steady state partial differential equation describing fluid flow in a fracture with spatially variable aperture (Abdel-Salam and Chrysikopoulos, 1995b)

$$\frac{\partial}{\partial x}\left[b^3(x, y)\frac{\partial h(x, y)}{\partial x}\right] + \frac{\partial}{\partial y}\left[b^3(x, y)\frac{\partial h(x, y)}{\partial y}\right] = 0. \tag{37}$$

The preceding equation is valid when the curvature of the fracture is small (Reimus *et al.*, 1995), and is derived under the assumption that the cubic law for incompressible laminar flow between two parallel plates (Schrauf and Evans, 1986) can simulate efficiently the flow through each unit element of the fracture. Flow in the rock matrix is neglected, because the saturated hydraulic conductivity in the rock matrix is several orders of magnitude smaller than the saturated hydraulic conductivity in the fracture (Streltsova, 1988). It should be noted that both the governing colloid transport equation (26) and the interstitial fluid flow equation (37) are stochastic partial differential equations because b is a stochastic variable.

The boundary conditions imposed on the two-dimensional fracture for the interstitial fluid flow model are:

$$\frac{\partial h(t, x, 0)}{\partial y} = 0, \tag{38}$$

$$\frac{\partial h(t, x, \ell_y)}{\partial y} = 0, \tag{39}$$

$$h(t, 0, y) = h_0, \tag{40}$$

$$h(t, \ell_x, y) = 0, \tag{41}$$

where h_0 is a constant total head potential. Conditions (38) and (39) represent the no flow top and bottom boundaries, respectively; whereas conditions (40) and (41) represent the constant head left (upstream) and right (downstream)

boundaries, respectively (for physical orientation of the fracture see Figure 5). The direction of the flow is from left to right. Figure 6 shows a plot of the velocity vector field in the fracture plane for a single realization of the aperture field obtained by solving eqn (37) subject to conditions (38)–(41) using the central finite difference approximation as outlined by Huyakorn and Pinder (1983) and Strikwerda (1989). The constant head gradient imposed on the flow model is 3.0×10^{-5}. This value represents a 1.72 m/y velocity in a fracture with constant aperture of 45 μm (this is the mean of the assumed lognormal distribution). The length of each arrow is proportional to the magnitude of the resultant velocity, with values ranging between 0.4–4.0 m/y. Velocities below 0.4 m/y and above 4.0 m/y are not shown. Since the velocity is proportional to the aperture squared and the head gradient, high velocities are found within elements with large aperture size and/or large head gradient.

Although microscopically the deposition of colloids is affected by many physicochemical processes, in order to model macroscopic colloid transport the following phenomenological equation describing the mass flux of colloids onto the fracture surfaces is used

$$\frac{\partial n^*(t, x, y)}{\partial t} = \kappa \left(U_x^2 + U_y^2\right)^{1/2} \frac{n(t, x, y)}{b(x, y)}. \tag{42}$$

The above equation is a modified version of eqn (2) which is applicable to fractures with uniform unidirectional interstitial velocity. One of the limitations of (42) is that it does not account for the reduction in fracture permeability as a result of colloid deposition onto fracture surfaces. This issue is explored in the next section of this chapter.

3.2 Colloid size exclusion

For each realization of the aperture field, the distribution of the total head potential (h) within the fracture is determined. Subsequently, the velocity components at each unit element of the fracture plane are obtained from (35) and (36) with $\gamma = 9.778 \times 10^6$ g $\cdot$ m^{-2}sec^{-2} and $\mu = 0.8904$ g $\cdot$ m^{-1}sec^{-1}. The corresponding hydrodynamic dispersion coefficients at each unit element are estimated by employing (29). Furthermore, the governing transport partial differential equation (26) coupled with the kinetic colloid deposition model (42) is solved numerically
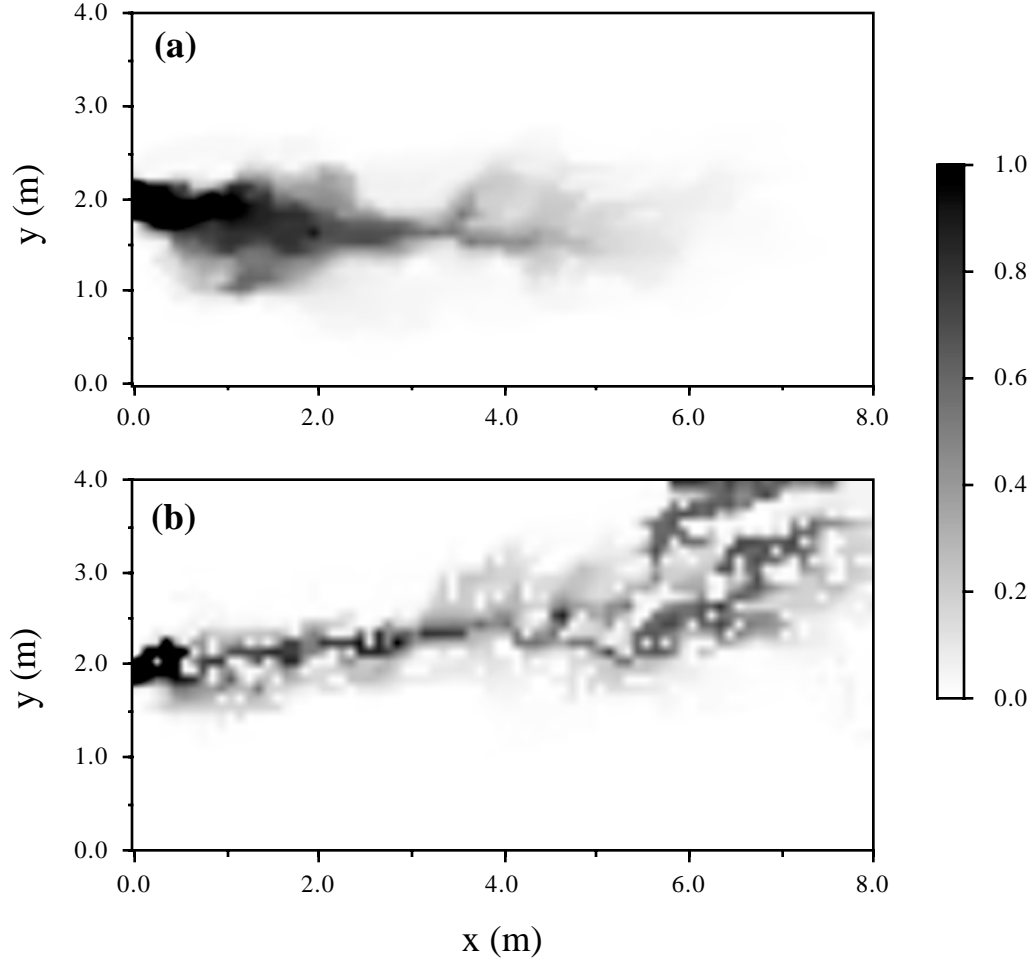
Figure 7: Spatial distribution of normalized suspended colloid concentration in the fracture plane, for transport: (a) without size exclusion and (b) with size exclusion. The colloid source is 0.4 m wide at the center of the inlet boundary (here $K_f = 1.0 \times 10^{-4}$ m, $t = 6$ y, $\alpha_L = 0.2$ m, and $\alpha_T = 0.02$ m).

subject to initial/boundary conditions (30)–(34) by employing the fully implicit finite difference method, as outlined by Huyakorn and Pinder (1983) and Strikwerda (1989). The time derivative is approximated by a two-point backward finite difference scheme and the spatial derivatives are approximated by a central finite difference scheme. The overall approximation is second-order accurate.

For fractures with spatially variable aperture, it is expected that colloids will bypass small size elements by following the least resistive pathways. This phenomenon is known as size exclusion. Figure 7 shows a comparison between colloid concentration in the fracture plane with and without size exclusion for a single realization after six years of simulation time. The colloid source is 0.4 m wide located at the center of the inlet boundary. The scale in Figure 7 ranges from black representing high concentration (n/n_o=1) to white representing low concentration (n/n_o=0). The two-dimensional snapshot in Figure 7a portrays the colloid concentration where colloids are allowed to travel throughout the whole fracture plane. Because of the variable aperture nature of the fracture, formation of some fingering occurs. In Figure 7b, colloids are restricted from entering elements with apertures smaller than 15 μm, assuming that colloid particles are spherical and of equal diameter (1 μm) so that the possibility of particle straining is eliminated (Sakthivadivel, 1969; Herzig et $al.$, 1970). No-flow elements are simulated by setting both the advective and dispersive fluxes into these elements to zero. It is clear from Figure 7b that size exclusion leads to faster breakthrough and more pronounced fingering. The small white spots in Figure 7b represent the no-flow elements.

4 Colloid deposition

For time dependent colloid deposition in a saturated fracture, under the assumption that the colloid filtration theory (Herzig et $al.$, 1970) is applicable, the following kinetic deposition model can be used (Chrysikopoulos and Abdel-Salam, 1997)

$$\frac{\partial n^*(t,x,y)}{\partial t} = r_f \frac{n(t,x,y)}{b(x,y)} - r_r n^*(t,x,y), \tag{43}$$

where r_f and r_r are the forward and reverse colloid deposition rate coefficients, respectively. This relationship for the kinetic colloid deposition onto fracture surfaces is more general than the expressions (2) and (42), because neither surface exclusion nor colloid deposition effects are neglected. The forward rate coefficient is defined as

$$r_f = \kappa \left(U_x^2 + U_y^2 \right)^{1/2} F(n^*), \tag{44}$$

where $F(n^*)$ is the dynamic blocking function (DBF), which takes into account the effect of previously deposited particles on subsequent colloid deposition by

specifying the portion of the fracture surface area available for deposition (surface exclusion effect). The DBF depends on the shape and size of colloids, geometry of sorbent, flow characteristics, and physicochemical properties of the interstitial fluid. The value of the DBF ranges between one for a fracture surface free of colloids ($n^* = 0$) and zero for a fracture surface completely covered (monolayer) by deposited colloids ($n^* = n^*_{\max}$, where $n^*_{\max}$ is the maximum deposited colloid concentration). A linear (Langmuirian) DBF as well as several nonlinear DBFs have been proposed in the literature for a variety of physical systems.

The colloid deposition coefficient κ presented in the expression describing the forward rate coefficient (44) can be approximated for cases of ideal flow conditions and collectors of regular geometrical shape (i.e., rotating disk, spherical and cylindrical collectors, a plate in a uniform flow, parallel-plate channel, and continuous moving surfaces) (van de Ven, 1989; Elimelech *et al.*, 1995). For natural subsurface formations or for the fracture with spatially variable aperture, the mechanisms controlling the colloid deposition coefficient are, in general, very complex and depend on the nature of the collector surface. Any kind of surface roughness or spatial variability of the surface charge can substantially affect colloid deposition. Because of inadequate information to predict in advance colloid deposition onto the fracture walls, the deposition coefficient is often considered a lumped parameter.

4.1 Linear DBF

The Langmuirian dynamic blocking function, which is linearly dependent on colloid surface coverage, has been used by many investigators (Privman *et al.*, 1991; Ryde *et al.*, 1991; Saiers *et al.*, 1994; Song and Elimelech, 1994, to mention a few representative studies) and is expressed as follows

$$F(n^*) = \frac{\epsilon_{\max} - \epsilon}{\epsilon_{\max}}, \tag{45}$$

where ϵ and $\epsilon_{\max}$ are the fraction and maximum fraction of a sorbent surface covered (blocked) by deposited colloids, respectively. It should be noted that $\epsilon_{\max}$ corresponds to the maximum deposited colloid concentration ($n^*_{\max}$), which is a function of colloidal particle size and available sites for colloid deposition. The preceding relationship incorporates blocking effects due to physical coverage of the sorbent's surface area by previously deposited colloids, as well as for possible additional inhibition of subsequent colloid deposition (blocking greater than the projected or cross-sectional area of the deposited colloid) due to energy barriers created by electrostatic repulsive forces originating from charged deposited colloids.

4.2 Nonlinear DBF

Schaaf and Talbot (1989) developed a DBF based on the random sequential adsorption (RSA) process which is governed by irreversible deposition without surface diffusion and colloidal particle overlapping (i.e., monolayer coverage). The RSA DBF was derived by considering the probability of a spherical particle to deposit on a flat surface with previously deposited particles present, and is valid only for uncharged colloidal particles at the maximum surface coverage possible of $\epsilon_{\max}$ =0.546. An improved, more flexible version of this DBF was presented by Adamczyk et $al.$ (1992), and is given as

$$F(n^*) = 1 - 2.184 \left[\frac{\epsilon}{\epsilon_{\max}} \right] + 0.986 \left[\frac{\epsilon}{\epsilon_{\max}} \right]^2 + 0.229 \left[\frac{\epsilon}{\epsilon_{\max}} \right]^3. \tag{46}$$

The preceding equation is a nonlinear function of the colloid surface coverage, and is valid for charged colloidal particles and any surface coverage up to 0.8 $\epsilon_{\max}$. For higher surface coverage, the following relationship can be used (Pomeau, 1980)

$$F(n^*) = \frac{\left(\epsilon_{\max} - \epsilon \right)^3}{2k^2}, \tag{47}$$

where k is an empirical parameter dependent on the area blocked by a single deposited particle.

4.3 Deposition model parameter estimation

In order to estimate the portion of a fracture surface area covered by colloids (ϵ), the number of deposited particles per unit surface area of the fracture (N^*) is obtained from the deposited colloid concentration (n^*) by the following expression

$$N^*(t, x, y) = \frac{n^*(t, x, y)}{\rho_p V_p}$$
$$= \frac{6n^*(t, x, y)}{\rho_p \pi d_p^3}, \tag{48}$$

where ρ_p is the colloidal particle density; $V_p = \pi d_p^3/6$ is the volume of a spherical colloidal particle; and d_p is the diameter of a colloidal particle. The preceding

equation transforms the deposited mass concentration to particle number concentration. The maximum number of particles which can possibly deposit on a fracture surface area is defined by

$$N^*_{\max} = \frac{1}{\alpha}, \tag{49}$$

where α is the area of the fracture surface blocked by a deposited colloidal particle. The parameter α is proportional to the projected (cross-sectional) area of a colloidal particle ($A_p = \pi d_p^2/4$) and is given by

$$\alpha = \beta A_p$$
$$= \beta \left(\frac{\pi d_p^2}{4} \right), \tag{50}$$

where β is the excluded area factor, which is a dimensionless parameter representing the ratio of the fracture surface area blocked by a deposited colloidal particle to the projected area of the particle ($\beta \geq 1$ and $\alpha \geq A_p$). In view of eqns (48)–(50), the portion of a fracture surface area blocked by colloids is evaluated as

$$\epsilon(t, x, y) = \frac{A_p N^*(t, x, y)}{\alpha N^*_{\max}}$$
$$= \frac{3}{2} \frac{n^*(t, x, y)}{\rho_p d_p}. \tag{51}$$

The maximum fraction of a fracture surface area blocked by deposited colloids is obtained by replacing N^* with $N^*_{\max}$ in (51) to yield

$$\epsilon_{\max} = \frac{A_p}{\alpha}$$
$$= \frac{1}{\beta}, \tag{52}$$

where the latter formulation in the preceding equation is the consequence of employing the definition of α.
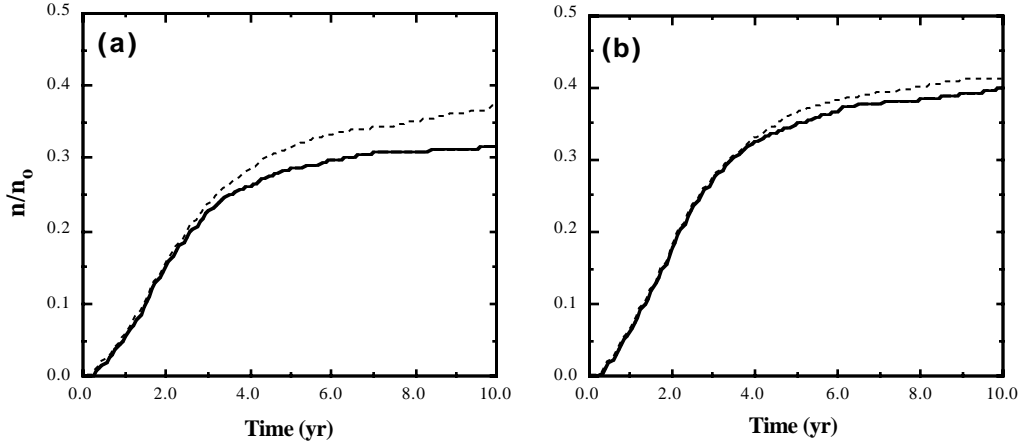
Figure 8: Comparison between normalized ensemble averaged temporal distribution of liquid phase colloid concentration for irreversible colloid deposition conditions with linear DBF (dashed curves) and clean bed media assumption (solid curves) for deposition coefficient of: (a) $\kappa=1.0\times10^{-9}$ m and (b) $\kappa=5.0\times10^{-10}$ m (here $d_p=1.0$ μm, $x=2.0$ m).

4.4 Effects of irreversible and reversible colloid deposition

When interstitial fluid and sorbent surface chemical conditions favor the presence of stable colloidal particles of opposite charge to sorbent surfaces, colloid deposition is essentially irreversible (i.e., $r_r=0$) and restricted to monolayer coverage of sorbent surfaces (Johnson and Elimelech, 1995). For this case, the expression (43) is employed with zero reverse rate coefficient. Furthermore, the forward colloid deposition rate coefficient is defined by (44) and $F(n^*)$ is described either by the linear relationship (45) or the nonlinear model (46)–(47).

The effect of irreversible colloid deposition described by the linear DBF (45) on colloid transport for particles of 1.0 μm in diameter is illustrated in Figure 8. The solid curves represent the clean bed media assumption (i.e., $F(n^*)=1$) for which colloid deposition is unaffected by previously deposited particles (Herzig et al., 1970); whereas the dashed curves represent the linear DBF. An ensemble average of 60 different realizations for a deposition coefficient of $\kappa = 1.0\times10^{-9}$ m
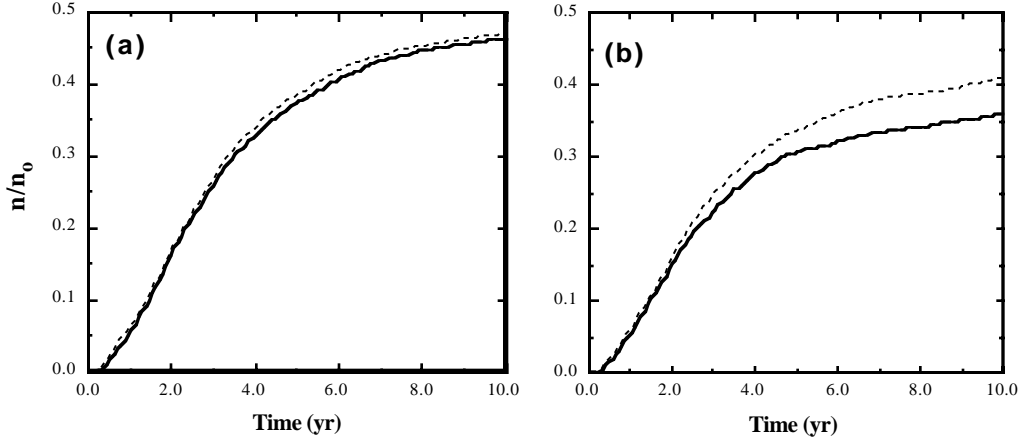
Figure 9: Comparison between normalized ensemble averaged temporal distribution of liquid phase colloid concentration for reversible colloid deposition conditions with linear DBF (dashed curves) and clean bed media assumption (solid curves) for reverse rate coefficient of: (a) r_r=1.0 yr^{-1} and (b) r_r=0.1 yr^{-1} (here d_p=1.0 μm, κ=1.0×10^{-9} m, $x = 2.0$ m).

and a source colloid concentration distributed across the entire width of the inlet boundary is presented in Figure 8a. The rising portion of the two breakthrough curves in Figure 8a coincide, because at early times the deposited colloid concentration is small ($\epsilon \rightarrow 0$) and the linear DBF is essentially one. With increasing time, progressive deviation between the two curves is observed. As the portion of the fracture surface covered by deposited colloids increases ($\epsilon > 0$), the DBF decreases, and the rate of colloid deposition declines; consequently, the liquid-phase colloid concentration increases. In Figure 8b, a smaller deposition coefficient ($\kappa = 5.0 \times 10^{-10}$ m) is employed. Comparing Figures 8a and 8b, it is evident that the rising portion of the breakthrough curve for the linear DBF coincides with the curve corresponding to the case of $F(n^*) = 1$ for longer periods of time. At late times the deviation of the breakthrough curves is less pronounced for the case of a smaller colloid deposition coefficient.

Comparing model simulations based on the nonlinear DBF (46)–(47) and linear DBF (45) it was concluded that at early times, the linear and nonlinear DBFs are essentially equivalent because the deposited colloid concentration is small. As the deposited colloid concentration increases, the RSA DBF yields

higher liquid phase colloid concentrations. Therefore, the colloid deposition rate is declining faster for the RSA DBF than the linear DBF.

Simulated breakthrough curves for an ensemble average of 60 realizations of the fracture aperture distribution, and for a source of colloids located across the entire width of the inlet boundary, is shown in Figure 9a for r_r=1 yr^{-1}. The solid curve is for the case where the clean bed media assumption is invoked; whereas the dashed curve is for the case where the linear DBF (45) is used. The nonlinear RSA DBF is not employed because it accounts for only irreversible colloid deposition. The two breakthrough curves presented in Figure 9a exhibit very similar behavior, because the effect of the linear DBF in decreasing the colloid deposition rate is insignificant due to the high reverse rate coefficient used, or equivalently, to the low deposited colloid concentration. In Figure 9b, a reverse rate coefficient of r_r =0.1 yr^{-1} is used. Clearly, for this case the two breakthrough curves progressively deviate from each other with increasing time. The lower reverse rate coefficient yields higher deposited colloid concentrations. Consequently, the effect of the linear DBF in decreasing the colloid deposition rate is more pronounced due to increased coverage of fracture surfaces by previously deposited colloids.

5 Summary

One-dimensional colloid transport in a single semi-infinite fracture idealized as two parallel plates was modeled assuming irreversible deposition onto fracture surfaces, penetration into the rock matrix, and irreversible deposition onto rock-matrix solid surfaces. Several analytical solutions corresponding to colloid transport with and without penetration into the rock matrix were presented, for constant concentration as well as constant flux inlet boundary conditions. The liquid phase colloid concentration in the fracture was found to be mostly sensitive to the fracture aperture and to the fracture surface deposition coefficient. An increase in the deposition coefficient produces an increase in the deposited colloid concentration on fracture surfaces and consequently a decrease in the liquid phase colloid concentration. As the fracture aperture decreases the liquid phase colloid concentration declines sharply, while the deposited colloid concentration on fracture surfaces increases. Simulations based on the analytical solutions for the case where colloids penetrate the rock matrix indicate an increase in the colloidal mass flux penetrating the rock matrix with decreasing particle size, which in turn leads to a reduction in the liquid phase colloid concentration in the fracture.

For the case of colloid transport in a two-dimensional fracture-rock matrix system with a spatially variable aperture and homogeneous, isotropic rock matrix, the model simulations suggest that colloid spreading increases when fracture aperture variability and size exclusion are considered, with the latter being important for large particles. Several model simulations indicate that a fracture with spatially variable aperture causes the colloids to follow preferential paths within the fracture plane. Faster transport and more pronounced fingering of colloids are observed when colloids are excluded from elements in the fracture plane with small aperture size. Size exclusion also increases the dispersion of colloids.

Incorporating a DBF in the deposition model leads to higher liquid phase colloid concentrations than what is predicted by the clean bed media assumption ($F(n^*) = 1$). The reason for this is that DBFs account for blocking effects from previously deposited colloidal particles. The nonlinear DBF yields substantially higher liquid phase colloid concentrations than the linear DBF, because the nonlinear model declines faster with increasing deposited colloid concentration. The impact of the DBF in increasing the liquid phase colloid concentration becomes insignificant at high reverse rate coefficients. Although the equilibrium colloid deposition mechanism is mathematically simple, it should be used with caution because it may not always accurately represent the colloid deposition process in subsurface systems.

Acknowledgements

Notation

A_p	Projected (cross-sectional) area of a colloidal particle: $\pi d_p^2/4$, L^2
b	Fracture aperture, L
d_p	Diameter of a colloidal particle, L
D	Dispersion coefficient for colloids, L^2/T
D_{ij}	Hydrodynamic dispersion coefficient in the ij $(ij = xx, xy, yx, yy)$ direction, L^2/T

D	Hydrodynamic dispersion coefficient tensor, L^2/T
$\mathcal{D}$	Brownian diffusion coefficient for colloids, L^2/T
$\mathcal{D}_e$	Effective diffusion coefficient for colloids, L^2/T
erf[x]	Error function, equal to $2\pi^{-1/2}\int_0^x e^{-z^2}dz$
erfc[x]	Complementary error function, equal to $1 - \text{erf}[x]$
F	Dynamic blocking function
F	Arbitrary two-dimensional vector
h	Total head potential in the fracture, L
h_0	Constant total head potential at the upstream boundary, L
k	Empirical parameter that varies with α
J_1	Bessel function of the first kind of order one
K_f	Hydraulic conductivity of the fracture: $\gamma b^2/12\mu$, L/T
ℓ_x	Fracture length in the x direction, L
ℓ_y	Fracture length in the y direction, L
n	Liquid-phase colloid concentration in the fracture, M/L^3
n_m	Liquid-phase colloid concentration in the rock matrix, M/L^3
n_o	Source colloid concentration, M/L^3
n^*	Colloid concentration deposited on fracture surfaces, M/L^2
n_m^*	Colloid concentration deposited onto rock matrix solid surfaces, M/M
$n_{\max}^*$	Maximum deposited colloid concentration on the fracture surfaces, M/L^2
N^*	Number of colloidal particles per unit surface area of the fracture, $1/L^2$
$N_{\max}^*$	Maximum number of deposited colloids per unit surface area of the fracture, $1/L^2$
r_f	Forward colloid deposition rate coefficient, $1/T$
r_r	Reverse colloid deposition rate coefficient, $1/T$
t	Time, T
U_x	Interstitial velocity in the x direction, L/T
U_y	Interstitial velocity in the y direction, L/T
U	Interstitial velocity vector, L/T
V_p	Volume of a spherical colloidal particle: $\pi d_p^3/6$, L^3
x	Coordinate along the fracture axis, L
y	Coordinate along the fracture width, L
z	Coordinate perpendicular to the fracture axis, L

Greek Letters

α	Fracture surface area blocked by a deposited colloidal particle, L^2
α_L	Longitudinal dispersivity, L

α_T	Transverse dispersivity, L
β	Excluded area factor
γ	Specific weight of the interstitial fluid, M/L^2T^2
δ_{ij}	Kronecker delta
ϵ	Fraction of a fracture surface area blocked by deposited colloids
$\epsilon_{\max}$	Fraction of a fracture surface area blocked by deposited colloids when n^* reaches $n^*_{\max}$
η	Dummy integration variable
θ	Porosity of the rock (liquid volume/rock matrix volume), L^3/L^3
κ	Fracture surface deposition coefficient, L
κ_m	Rock matrix deposition coefficient, 1/T
μ	Dynamic viscosity of the interstitial fluid, M/LT
ν	Dummy integration variable
ξ	Defined in (10)
ρ_b	Bulk density of the rock matrix, M/L^3
ρ_p	Colloidal particle density, M/L^3
τ	Dummy integration variable
τ^*	Rock matrix tortuosity
ω	Dummy integration variable

Subscripts

cc	Constant concentration boundary condition without colloid penetration into the rock matrix
cc_p	Constant concentration boundary condition with colloid penetration into the rock matrix
cf	Constant flux boundary condition without colloid penetration into the rock matrix
cf_p	Constant flux boundary condition with colloid penetration into the rock matrix

Abbreviations

DBF	Dynamic blocking function
RSA	Random sequential adsorption

References

Abdel-Salam, A., and C. V. Chrysikopoulos, Analytical solutions for one-dimensional colloid transport in saturated fractures, *Advances in Water Resour.*, **17**, 283–296, 1994.

Abdel-Salam, A., and C. V. Chrysikopoulos, Analysis of a model for contaminant transport in fractured media in the presence of colloids. *J. Hydrol.,* **165**, 261–281, 1995a.

Abdel-Salam, A., and C. V. Chrysikopoulos, Modeling of colloid and colloid-facilitated contaminant transport in a two-dimensional fracture with spatially variable aperture, *Transp. Porous Media*, **20**, 197–221, 1995b.

Abelin, H., Migration in a single fracture: An in situ experiment in a natural fracture. Ph.D. dissertation, Dep. of Chem. Eng., R. Inst. of Tech., Stockholm, 170 pp., 1986.

Adamczyk, Z., B. Siwek, and M. Zembala, Reversible and irreversible adsorption of particles on homogeneous surfaces, *Colloids and Surf.*, **62**, 119–130, 1992.

Adamczyk, Z., B. Siwek, M. Zembala, and P. Belouschek, Kinetics of localized adsorption of colloid particles, *Adv. Colloid and Interface Sci.*, **48**, 151–280, 1994.

Bear, J., and A. Verruijt, *Modeling Groundwater Flow and Pollution*, Reidel, Dordrecht, Holland, 1987.

Bianchi, L., and D. Snow, Permeability crystalline rock interpreted from measured orientations and apertures of fractures, *Annu. Arid Zone*, **8**, 231–245, 1968.

Birgersson, L., and I. Neretnieks, Diffusion in the matrix of granitic rock field test in the Stripa mine, Part 1, SKBF/KBS Teknish Rapport, 82–08, Royal Inst. Technol., Stockholm, Sweden, 1982.

Bourke, P. J., E. M. Dunance, M. J. Heath, and D. D. Hodgkinson, Fracture hydrology relevant to radionuclide transport, AERE Rep. 11414, Atomic Energy Res. Estab., Harwell, United Kingdom, 1985.

Bowen, B. D., and N. Epstein, Fine particle deposition in smooth parallel-plate channels, *J. Colloid Interface Sci.*, **72**, 81–97, 1979.

Buddemeier, R. W., and J. R. Hunt, Transport of colloidal contaminants in groundwater radionuclide migration at the Nevada test site, *Applied Geochemistry*, **3**, 535–548, 1988.

Champ, D. R., and J. Schroeter, Bacterial transport in fractured rock: A field-scale tracer test at the Chalk River Nuclear Laboratories, *Water Sci. Technol.*, **20**, 81–87, 1988.

Chiou, C. T., R. L. Malcom, T. I. Brinton, and D. E. Kile, Water solubility enhancement of some organic pollutants and pesticides by dissolved humic and fulvic acids, *Environ. Sci. Technol.*, **20**, 502–508, 1986.

Chrysikopoulos, C. V., and Y. Sim, One-dimensional virus transport in homogeneous porous media with time-dependent distribution coefficient, *J. Hydrol.*, **185**, 199–219, 1996.

Chrysikopoulos, C. V., and A. Abdel-Salam, Modeling colloid transport and deposition in saturated fractures, *Colloids Surfaces A: Physicochem. Eng. Aspects*, **121**, 189–202, 1997.

de Marsily, G., *Quantitative Hydrogeology: Groundwater Hydrology for Engineers*, Academic Press, 440 pp., 1986.

Drever, J. I., *The Chemistry of Weathering*, Reidel Publishing Co., Dordrecht, Holland, 325 pp., 1985.

Elimelech, M., J. Gregory, X. Jia, and R. Williams, *Particle Deposition and Aggregation: Measurement, Modeling and Simulation*, Butterworth-Heinemann, Oxford, Great Britain, 1995.

Gale, J. E., The effects of fracture type (induced versus natural) on the stress–fracture closure–fracture permeability relationships, in *Proceedings at 23rd Symposium on Rock Mechanics*, Univ. Calif., Berkeley, 290–298, 1982.

Gershon, N. D., and A. Nir, Effects of boundary conditions of models on tracer distribution in flow through porous mediums, *Water Resour. Res.*, **4**, 830–839, 1969.

Goldman, A. J., R. G. Cox, and H. Brenner, Slow viscous motion of a sphere parallel to a plane wall – I: motion through quiescent fluid, *Chem. Eng. Sci.*, **22**, 637–651, 1967.

Grindrod, P., The impact of colloids on the migration and dispersal of radionuclides within fractured rock, *J. Contam. Hydrol.*, **13**, 167–181, 1993.

Hakami, E., and N. Barton, Aperture measurements and flow experiments using transparent replicas of rock joints, in *Rock Joints*, edited by N. Barton and O. Stephansson, A. A. Balkema, 383–390, 1990.

Harvey, R. W., and S. P. Garabedian, Use of colloid filtration theory in modeling movement of bacteria through a contaminated sandy aquifer, *Env. Sci. Technol.*, **25**, 178–185, 1991.

Herzig, J. P., D. M. Leclerc, and P. Le Goff, Flow of suspension through porous media: Application to deep filtration, *Ind. Eng. Chem.*, **62**, 9–35, 1970.

Huyakorn, P. S., and G. F. Pinder, *Computational Methods in Subsurface Flow*, Academic Press, 473 pp., 1983.

Ibaraki, M., and E. A. Sudicky, Colloid-facilitated contaminant transport in discretely fractured porous media, 1, Numerical formulation and sensitivity analysis, *Water Resour. Res.*, **31**, 2945–2960, 1995.

Johns, R. A., and P. V. Roberts, A solute transport model for channelized flow in a fracture, *Water Resour. Res.*, **27**, 1797–1808, 1991.

Johnson, P. R., and M. Elimelech, Dynamics of colloid deposition in porous media: blocking based on random sequential adsorption, *Langmuir*, **11**, 801–812, 1995.

Kessler, J. H., and J. R. Hunt, Dissolved and colloidal contaminant transport in a partially clogged fracture, *Wat. Resour. Res.*, **30**, 1195–1206, 1994.

Krishnamoorthy, T. M., R. N. Nair, and T. P. Sarma, Migration of radionuclides from a granite repository, *Water Resour. Res.*, **28**, 1927–1934, 1992.

Leij, F. J., T. H. Skaggs, and M. Th. van Genuchten, Analytical solutions for solute transport in three-dimensional semi-infinite porous media, *Water Resour. Res.*, **27**, 2719–2733, 1991.

Lindstrom, F. T., R. Haque, V. H. Freed, and L. Boersma, Theory on the movement of some herbicides in soils: Linear diffusion and convection of chemicals in soils, *Env. Sci. Technol.*, **1**, 561–565, 1967.

Matthess, G., and A. Pekdeger, Concepts of a survival and transport model of pathogenic bacteria and viruses in groundwater, *Sci. Tot. Env.*, **21**, 149–159, 1981.

Matthess, G., A. Pekdeger, and J. Schroeter, Persistence and transport of bacteria and viruses in groundwater: A conceptual evaluation, *J. Contam. Hydrol.*, **2**, 171–188, 1988.

McCarthy, J. F., and C. Degueldre, Sampling and characterization of colloids and particles in groundwater for studying their role in contaminant transport, in *Environmental Particles*, Vol. 2, edited by J. Buffle and H. P. van Leeuwen, pp. 247–315, 1993.

McCarthy, J. F., and J. M. Zachara, Subsurface transport of contaminants, *Env. Sci. Technol.*, **23**, 496–502, 1989.

McDowell-Boyer, L. M., J. R. Hunt, and N. Sitar, Particle transport through porous media, *Water Resour. Res.*, **22**, 1901–1921, 1986.

Mills, W. B., S. Liu, and F. K. Fong, Literature review and model (COMET) for colloid/metals transport in porous media, *Ground Water*, **29**, 199–208, 1991.

Mitchell, J. K., *Fundamentals of Soil Behavior*, John Wiley & Sons, 1976.

Moreno, L., Y. W. Tsang, C. F. Tsang, F. V. Hale, and I. Neretnieks, Flow and tracer transport in a single fracture: A stochastic model and its relation to some field observations, *Water Resour. Res.*, **24**, 2033–2048, 1988.

Moulin, V., and G. Ouzounian, Role of colloids and humic substances in the transport of radio-elements through the geosphere, *Applied Geochemistry, Suppl. Issue* (1), 179–186, 1992.

Neretnieks, I., A note on fracture flow dispersion mechanisms in the ground, *Water Resour. Res.*, **23**, 561–570, 1983.

Neretnieks, I., T. Eriksen, and P. Tahtinen, Tracer movement in a single fissure in granitic rock: Some experimental results and their interpretation, *Water Resour. Res.*, **18**, 849–858, 1982.

Neuzil, C. E., and J. V. Tracy, Flow through fractures, *Water Resour. Res.*, **17**, 191–199, 1981.

Novakowski, K. S., G. V. Evans, D. A. Lever, and K. Raven, A field example of measuring hydrodynamic dispersion in a single fracture, *Water Resour. Res.*, **21**, 1165–1174, 1985.

Pomeau, Y., Some asymptotic estimates in the random parking problem, *J. Phys. A: Math. Gen.*, **13**, 193–196, 1980.

Privman, V., H. L. Frisch, N. Ryde, and E. Matijevic, Particle adhesion in model systems: 13, Theory of multilayer deposition, *J. Chem. Soc. Faraday Trans.*, **87**, 1371–1375, 1991.

Puls, R. W., and R. M. Powell, Transport of inorganic colloids through natural aquifer material: Implications for contaminant transport, *Env. Sci. Technol.*, **26**, 614–621, 1992.

Raven, K. G., K. S. Novakowski, and P. A. Lapeciv, Interpretation of field tracer tests of a single fracture using a transient solute storage model, *Water Resour. Res.*, **24**, 2019–2032, 1988.

Reimus, P. W., B. A. Robinson, H. E. Nuttall, and R. Kale, *Mat. Res. Soc. Symp. Proc.*, **353**, 363–369, 1995.

Russel, W. B., D. A. Saville, and W. R. Schowalter, *Colloidal Dispersions*, Cambridge, Great Britain, 525 pp., 1989.

Ryde, N., N. Kallay, and E. Matijevic, Particle adhesion in model systems, 14, Experimental Evaluation of multilayer deposition, *J. Chem. Soc. Faraday Trans.*, **87**, 1377–1381, 1991.

Saiers, J. E., G. M. Hornberger, and L. Liang, First– and Second–order approaches for modeling the transport of colloidal particles in porous media, *Water Resour. Res.*, **30**, 2499-2506, 1994.

Sakthivadivel, R., Clogging of a granular porous medium by sediment, Hydraul. Eng. Lab., Univ. of Calif., Berkeley, *Report HEL 15-17*, 106 pp., 1969.

Schaaf, P., and J. Talbot, Surface exclusion effects in adsorption processes, *J. Chem. Phys.*, **91**, 4401–4409, 1989.

Schrauf, T. W., and D. D. Evans, Laboratory studies of gas flow through a single natural fracture, *Water Resour. Res.*, **22**, 1038–1050, 1986.

Shapiro, A. M., and J. R. Nicholas, Estimating the statistical properties of fracture aperture using field scale hydraulic and tracer tests: Theory and application, *Water Resour. Res.*, **25**, 817–828, 1989.

Smith, P. A., and C. Degueldre, Colloid–facilitated transport of radionuclides through fractured media, *J. Contam. Hydrol.*, **13**, 143–166, 1993.

Song, L., and M. Elimelech, Transient deposition of colloidal particles in heterogeneous porous media, *J. Colloid Interface Sci.*, **167**, 301–313, 1994.

Streltsova, T. D., *Well Testing in Heterogeneous Formations*, Wiley, New York, 413 pp., 1988.

Strikwerda, J. C., *Finite Difference Schemes and Partial Differential Equations*, Wadsworth & Brooks/Cole, 386 pp., 1989.

Stumm, W., Chemical interaction in particle separation, *Env. Sci. and Technol.*, **11**, 1066–1070, 1977.

Stumm, W., and J. J. Morgan, *Aquatic Chemistry*, 2nd ed. Wiley, New York, 780 pp., 1981.

Tim, U. S., and Mostaghimi, S., Model for predicting virus movement through soils, *Ground Water*, **29**, 251–259, 1991.

Toran, L., and A. V. Palumbo, Colloid transport through fractured and unfractured laboratory sand columns, *J. Contam. Hydrol.*, **9**, 289–303, 1992.

Torok, J., L. P. Buckley, and B. L. Woods, The separation of radionuclide migration by solution and particle transport in soil, *J. Contam. Hydrol.*, **6**, 185–203, 1990.

Tsang, Y. W., and C. F. Tsang, Channel model of flow through fractured media, *Water Resour. Res.*, **23**, 467–479, 1987.

van de Ven, T. G. M., *Colloidal Hydrodynamics*, Academic Press, London, Great Britain, 1989.

van Genuchten, M. Th., and J. C. Parker, Boundary conditions for displacement experiments through short laboratory soil columns, *Soil Sci. Soc. Am. J.*, **48**, 703–708, 1984.

Williams, S. A., and A. I. El-Kadi, COVAR: A computer program for generating two-dimensional fields of autocorrelated parameters by matrix decomposition, Int. Groundwater Model. Center, Holcomb Research Inst., Colorado School of Mines, Golden, CO, 1986.